^{17}O MAS NMR Correlation Spectroscopy at High Magnetic Fields

Eric G. Keeler,[†,§] Vladimir K. Michaelis,[†,⊥] Michael T. Colvin,[†,∥] Ivan Hung,[‡] Peter L. Gor'kov,[‡] Timothy A. Cross,[‡] Zhehong Gan,[‡] and Robert G. Griffin*[,†]

[†]Department of Chemistry and Francis Bitter Magnet Laboratory, Massachusetts Institute of Technology, Cambridge, Massachusetts 02139, United States

[‡]National High Magnetic Field Laboratory, Florida State University, Tallahassee, Florida 32310, United States

S *Supporting Information*

ABSTRACT: The structure of two protected amino acids, FMOC-L-leucine and FMOC-L-valine, and a dipeptide, *N*-acetyl-L-valyl-L-leucine (N-Ac-VL), were studied via one- and two-dimensional solid-state nuclear magnetic resonance (NMR) spectroscopy. Utilizing ^{17}O magic-angle spinning (MAS) NMR at multiple magnetic fields (17.6−35.2 T/750−1500 MHz for ^{1}H) the ^{17}O quadrupolar and chemical shift parameters were determined for the two oxygen sites of each FMOC-protected amino acids and the three distinct oxygen environments of the dipeptide. The one- and two-dimensional, ^{17}O, $^{15}N-^{17}O$, $^{13}C-^{17}O$, and $^{1}H-^{17}O$ double-resonance correlation experiments performed on the uniformly $^{13}C,^{15}N$ and 70% ^{17}O-labeled dipeptide prove the attainability of ^{17}O as a probe for structure studies of biological systems. $^{15}N-^{17}O$ and $^{13}C-^{17}O$ distances were measured via one-dimensional REAPDOR and ZF-TEDOR experimental buildup curves and determined to be within 15% of previously reported distances, thus demonstrating the use of ^{17}O NMR to quantitate interatomic distances in a fully labeled dipeptide. Through-space hydrogen bonding of N-Ac-VL was investigated by a two-dimensional ^{1}H-detected ^{17}O R³-R-INEPT experiment, furthering the importance of ^{17}O for studies of structure in biomolecular solids.
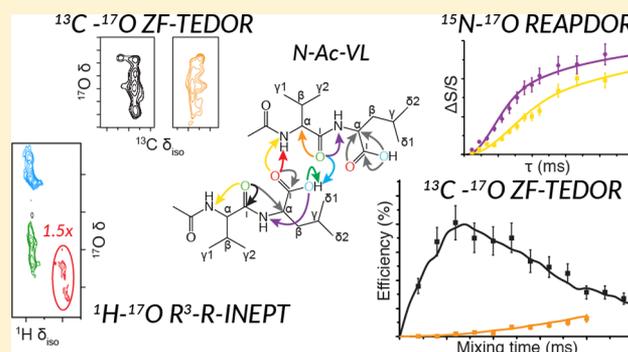
1. INTRODUCTION

The essential role of oxygen in hydrogen bonding in determining the chemistry, structure, and function of peptides and proteins is well known. It is also axiomatic that ^{17}O magic-angle spinning (MAS) nuclear magnetic resonance (NMR) experiments can in principle elucidate the details of these interactions via site-specific measurements of the chemical shift and quadrupole tensors. Furthermore, if a method of dipolar recoupling is included in the experimental protocol, then $^{13}C-^{17}O$ and $^{15}N-^{17}O$ and $^{1}H-^{17}O$ distance measurements and 3D structures are possible.[1,2] Nevertheless, the potential of ^{17}O NMR to provide this level of detailed structural information has never been realized primarily for three reasons: (i) ^{17}O is present with a low natural isotopic abundance (0.037%), (ii) it is a low gyromagnetic ratio nuclear spin ($\gamma = -5.774$ MHz T^{-1}), and (iii) it is a quadrupolar nucleus ($I = 5/2$). Thus, at ubiquitous magnetic fields ($\leq 5-14.1$ T, $\omega_{0H}/2\pi = 200-600$ MHz) the sensitivity observed in MAS NMR spectra is inherently low, and the resolution is low due to the residual second-order quadrupolar broadening that is not eliminated by magic-angle spinning.[3]

The direct solution to the first issue is isotopic enrichment and a relatively new solution to this problem is discussed below. The second and third issues are most easily addressed by using new NMR methods and by performing ^{17}O spectroscopy at high magnetic fields, which we define as greater than 14.1 T.[4−13] In particular, we report here spectroscopy at high fields (17.6−35.2 T, $\omega_{0H}/2\pi = 750-1500$ MHz) which enhances overall sensitivity, but more importantly attenuates the broadening from second-order quadrupole coupling arising from the quadrupole coupling constant (C_Q) of 7−9 MHz observed for $C=^{17}O$ chemical environments.[14−16] For example, in spectra described below, the second-order powder patterns are narrowed to a few kHz, concurrently increasing the resolution of the spectra. With the emergence of NMR magnets fabricated from high-temperature superconductors that generate 28−35 T on the horizon, these sorts of experimental data should become relatively routine. Thus, the motivation of the results reported here is to demonstrate the potential for significant advances and applications of ^{17}O NMR spectroscopy.

Because of the improved sensitivity and resolution in high-field ^{17}O MAS NMR spectra, it becomes feasible to perform correlation experiments to determine spectral assignments and measure structural parameters with dipole recoupling experiments. Both homonuclear and heteronuclear MAS recoupling experiments are routinely used to study the structure of

Scheme 1. Isotopic Labeling of FMOC Amino Acids Using the Multiple-Turnover Reaction with 1-Ethyl-3-(3-dimethylaminopropyl)carbodiimide Hydrochloride (EDC·HCl)[59]
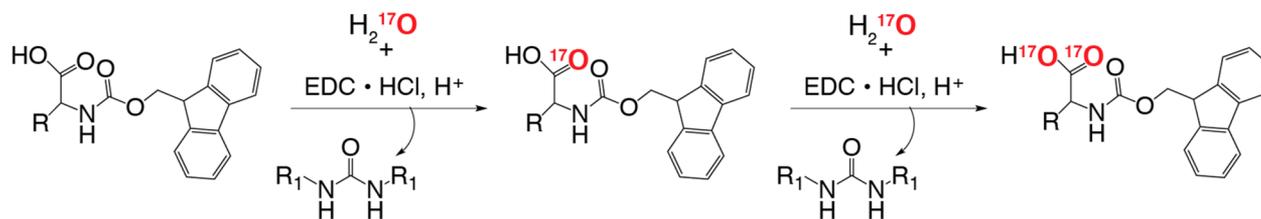
peptides and proteins,[17−20] and provide accurate measurements of $^{13}C-^{13}C$,[21−23] $^{13}C-^{15}N$,[24,25] and $^1H-^{13}C/^{15}N$[26−28] distances. This class of experiments is also applicable, with suitably modified pulse sequences, to $^{13}C-^{17}O$, $^{15}N-^{17}O$ and $^1H-^{17}O$ distance measurements; for example, heteronuclear recoupling experiments have been reported, although only a few examples of two-dimensional heteronuclear correlation experiments are in the literature.[29−35] $^{15}N-^{17}O$ rotational-echo adiabatic-passage double-resonance (REAPDOR)[36] experiments were used to examine hydrogen bonding in amyloid fibrils, with the most complete results requiring an isolated spin-pair and a determination of the precise level of ^{17}O enrichment in the sample to precisely measure the $^{15}N-^{17}O$ dipolar coupling.[4,29,37] Dipolar mediated heteronuclear correlation experiments between spin $I = 1/2$ and quadrupolar nuclei based on J-coupled experiments, such as rotary resonance recoupled (R^3) refocused insensitive nuclei enhanced by polarization transfer (R^3-R-INEPT), have been shown to produce high-efficiency polarization transfer.[30,38] The addition of a multiple-quantum (MQ) or satellite transition (ST) filter to the dipolar meditated heteronuclear experiments was shown to increase the resolution available in these experiments.[38] Finally, recent advances in ^{17}O spectroscopy including higher magnetic field experiments (>14.1 T),[4−13] application of population transfer techniques,[39−41] and dynamic nuclear polarization[31−33,42−44] enhance the ability to perform these distance measurements. Thus, successful ^{17}O studies of amino acids, polypeptides, pharmaceutical compounds, and amyloid fibrils have appeared in the literature using one or more of these strategies.[4−13,29,31−33,37,39−58]

Building on previous ^{17}O NMR experiments, we first describe an efficient procedure for ^{17}O labeling FMOC-protected amino acids using $H_2^{17}O$ as the source. The approach utilizes a nonequilibrium multiple-turnover reaction under mild and selective conditions.[59] Two FMOC-protected amino acid precursors, FMOC-L-valine and FMOC-L-lecuine, were ^{17}O enriched to 40 and 70%, with an efficiency of >95%, and used to prepare $[^{17}O/^{13}C/^{15}N]$-N-Ac-VL, a model dipeptide used to develop dipole recoupling experiments. We envision that these labeled amino acids can be used in contemporary peptide synthesis[60] or in cell-free synthesis protocols[61] for ^{17}O labeling of peptides and proteins.[4] Second, we recorded 1D MAS spectra at $\omega_{0H}/2\pi = 750$, 800, 900, and 1500 MHz and simulated the rotational sideband patterns to extract the chemical shift and electric field gradient (EFG) tensors for the three ^{17}O moieties: amide NC=O, carboxyl C=O, and C—OH. The C=^{17}O tensors have a span of 380−450 ppm and the C—^{17}OH span is 310−320; thus, the shift tensors are substantial and the shifts are very sensitive to chemical environment. The quadrupole coupling constants range between 7 and 8.5 MHz. Third, in order to demonstrate the utility of high magnetic fields in ^{17}O spectroscopy we

recorded 2D triple-quantum MAS (3QMAS) at 35.2 T ($\omega_{0H}/2\pi = 1.5$ GHz) for N-Ac-VL using the series-connected hybrid (SCH) magnet at the National High Magnetic Field Laboratory (NHMFL, Tallahassee, FL). At this field strength the second-order quadrupole powder patterns are reduced to ~2 kHz (~10 ppm), yielding excellent sensitivity and resolution. The 3QMAS experiment yields an isotropic dimension with the chemical and second-order quadrupole shift and an anisotropic dimension with the second-order line shapes and chemical shift information. Finally, using a variety of dipole recoupling techniques we measured a total of 14 $^{13}C-^{17}O$, $^{15}N-^{17}O$, and $^1H-^{17}O$ distances in *N*-acetyl-L-valyl-L-leucine (N-Ac-VL), demonstrating the viability of determining molecular structure with ^{17}O distance constraints.

2. EXPERIMENTAL SECTION

2.1. Materials and Synthesis. Traditionally ^{17}O enrichment of amino acids is performed via acid-catalyzed exchange at elevated temperature, where the amino acid is heated in the presence of strong acid and ^{17}O enriched water and yield enrichment efficiencies up to 85%.[62,63] These conditions prohibit acid-catalyzed exchange to be used for ^{17}O enrichment in protected amino acids or proteins, and therefore we have turned to an alternative procedure utilizing mild conditions and yielding $^{17}O/^{18}O$ isotopic enrichment efficiencies of >95%.[46,59,62−64] Utilizing this approach, illustrated in Scheme 1, FMOC-L-valine and FMOC-L-leucine were prepared using 40% $H_2^{17}O$ (Cambridge Isotope Laboratories, Andover, MA) for study via ^{17}O NMR spectroscopy. A dipeptide sample, $[^{17}O/^{13}C/^{15}N]$-N-Ac-VL, was prepared using the same approach with U-^{13}C,^{15}N amino acids and 70% $H_2^{17}O$ (Cambridge Isotope Laboratories, Andover, MA).

The following reagents were purchased from Sigma-Aldrich (St. Louis, MO), 1-ethyl-3-(3-(dimethylamino)propyl)carbodiimide hydrochloride (EDC·HCl), dimethylformamide (kept in a septum container), and 3,5-dimethylpyridine, which was then reacted with HBr (33% in acetic acid) to form 3,5-dimethylpyridine·HBr that was lyophilized to remove residual water. All starting materials were dried by preparing a sonicated suspension of each in acetonitrile, and removing residual water as an acetonitrile azeotrope by rotary evaporation. Drying was repeated in triplicate. Flame-dried glassware and stir bars were used and the reactions were carried out under dry Ar gas on a Schlenk line.

First, 430 mg of EDC·HCl (10 equiv) and 850 mg of dry 3,5-dimethylpyridine·HBr (20 equiv) were suspended in ~2−5 mL of DMF and added to 100 mg of FMOC-protected amino acid and 200 μL of 40% $H_2^{17}O$ (45 equiv) via a syringe. The reaction was stirred at room temperature for 18−24 h after which the reaction mixture was supplemented with 430 mg of EDC·HCl. This was repeated once and the reaction was allowed to stir for an additional 18−24 h. The reaction mixture was diluted with ~25 mL of ethyl acetate and dried with MgSO$_4$, washed three times with 0.1 M citric acid (~15 mL) and once with 0.1 M citric acid in brine (~15 mL) and filtered. The FMOC-protected amino acid products were purified by aqueous extraction with ethyl acetate (~25 mL) three times. The resulting solutions were lyophilized to yield pure FMOC-protected ^{17}O-labeled amino acids.

Table 1. NMR Acquisition Parameters for One-Dimensional ^{17}O Experiments

B_0 (T)	$\omega_0/2\pi$ (MHz)	pulse sequence	sample	$\omega_R/2\pi$ (kHz)	recycle delay (s)	scans (×1024)	^{1}H decouple
17.6	101.45	Hahn-echo	FMOC-L-leucine	15, 17, 18	0.3	63	no
				0	1.0	1340	yes
			FMOC-L-valine	18, 19, 20	0.3	63	no
				0	1.0	1340	yes
			N-Ac-VL	18, 20	0.3	63	no
				18	1.0	235	yes
18.8	108.36	Hahn-echo	FMOC-L-leucine	60	0.3	256	no
			N-Ac-VL	60	0.15	250	no
21.1	122.02	Hahn-echo	FMOC-L-leucine	24	0.25	20	no
			FMOC-L-valine	20	0.2	100	no
			N-Ac-VL	24	0.3	80	no
35.2	203.36	Hahn-echo	N-Ac-VL	19	0.1	4	no

Table 2. NMR Acquisition Parameters for Double Resonance and Two-Dimensional Experiments Involving ^{17}O

B_0 (T)	nuclei[a]	$\omega_0/2\pi$ (MHz)	pulse sequence	sample	$\omega_R/2\pi$ (kHz)	recycle delay (s)	scans	^{1}H decouple
17.6	^{1}H−^{17}O	749−101.45	R^3-R-INEPT	N-Ac-VL	20	0.1	4096	no
	^{15}N−^{17}O	76−101.45	REAPDOR	N-Ac-VL	18	3	256	yes
	^{15}N−^{17}O	76−101.45	ZF-TEDOR	N-Ac-VL	18	3	60416	yes
21.1	^{13}C−^{17}O	226.3−122.02	ZF-TEDOR	N-Ac-VL	20	3	512	yes
35.2	^{17}O	203.36	MATPASS	N-Ac-VL	19	0.1	1200	no
			3QMAS		19	0.2	1024	no

[a]Detection nucleus listed first.

Table 3. NMR Acquisition Parameters for One- and Two-Dimensional ^{1}H, ^{13}C, and ^{15}N Experiments

B_0 (T)	nucleus[a]	$\omega_0/2\pi$ (MHz)	pulse sequence	sample	$\omega_R/2\pi$ (kHz)	recycle delay (s)	scans	^{1}H decouple
11.7	^{13}C	125.3	CP MAS	FMOC-L-leucine	10	3	21280	yes
	^{13}C	125.3	CP MAS	FMOC-L-valine	10	3	18560	yes
	^{13}C	125.3	RFDR	N-Ac-VL	10	3	16	yes
	^{13}C−^{15}N	125.3−50.5	ZF-TEDOR	N-Ac-VL	10	3	256	yes
18.8	^{1}H	800	Bloch decay	N-Ac-VL	60	3	32	no
21.1	^{1}H	900.1	Bloch decay	N-Ac-VL	20	3	16	no
	^{13}C	226.3	CP MAS	N-Ac-VL	20	3	64	yes
	^{15}N	91.2	CP MAS	N-Ac-VL	20	3	256	yes

[a]Detection nucleus listed first.

In addition to the 40% ^{17}O-enriched FMOC-protected amino acids, [U-^{13}C,^{15}N]FMOC-L-valine and [U-^{13}C,^{15}N]FMOC-L-leucine were labeled with 70% ^{17}O H$_2$^{17}O (CIL, Andover, MA) using the procedure above. Finally, N-acetyl-[U-^{13}C,^{15}N,70% ^{17}O]-L-Val-L-Leu (N-Ac-VL) was synthesized by New England Peptide (Gardner, MA) using standard solid-phase methods and purified by high-performance liquid chromatography (HPLC).

The products were then recrystallized in dichloromethane (FMOC-L-valine), ethanol (FMOC-L-leucine), or water (N-Ac-VL) by slow evaporation. The ^{17}O labeling of each product was verified by mass spectrometry (Koch Institute MIT, FMOC amino acids; New England Peptide, N-Ac-VL).

2.2. Solid-State Nuclear Magnetic Resonance Spectroscopy. One- and two-dimensional ^{17}O NMR experiments were performed using a series of magnetic field strengths, all experimental parameters are summarized in Tables 1−3. Experiments at 21.1 T ($\omega_{0H}/2\pi$ = 900 MHz, FBML-MIT), were performed using a Bruker Avance II spectrometer and a 3.2 mm triple resonance (^{1}H, ^{13}C, ^{17}O) probe

(Bruker BioSpin, Billerica, MA, USA). Experiments at 18.8 T ($\omega_{0H}/2\pi$ = 800 MHz, FBML-MIT) were performed using a Bruker Avance III spectrometer and a 1.3 mm triple resonance (^{1}H, X, Y) probe (Bruker, BioSpin, Billerica, MA, USA). Experiments at 17.6 T ($\omega_{0H}/2\pi$ = 750 MHz, FBML-MIT) were performed using a home-built spectrometer (courtesy of Dr. David Ruben, FBML-MIT) and a 3.2 mm triple resonance (^{1}H, ^{17}O, ^{15}N) probe with a modified probe head employing a RevolutionNMR (Fort Collins, CO, USA) stator housing within a Bruker probe body. Additional ^{17}O NMR experiments were recorded on the 35.2 T ($\omega_{0H}/2\pi$ = 1500 MHz) series-connected hybrid magnet at the NHMFL[65] using a Bruker Avance NEO console and a single-resonance 3.2 mm MAS probe designed and constructed at the NHMFL. All ^{17}O NMR spectra were referenced to liquid water (18% H$_2$^{17}O) via the substitution method.[66] ^{17}O $\gamma B_1/2\pi$ varied between 83 and 156 kHz, and non-spinning experiments were acquired with continuous-wave high-power ^{1}H decoupling during acquisition ($\gamma B_1/2\pi$ = 100 kHz). We note that ^{1}H decoupling during acquisition of ^{17}O

Table 4. Amino Acid and Dipeptide ^{17}O NMR Parameters

sample	^{17}O site	δ_{iso} (ppm, ±1)	C_Q (MHz, ±0.2)	η_Q (±0.1)	Ω (±75)	κ (±0.25)	α (±20°)	β (±20°)	γ (±20°)
FMOC-L-leucine	CO	338	8.3	0.0	385	0.1	30	90	0
	COH	161	7.3	0.2	320	−0.8	20	65	70
FMOC-L-valine	CO	337	8.4$_5$	0.0	340	0.2	45	90	0
	COH	169	7.2$_5$	0.1$_5$	320	−0.7	20	65	70
N-Ac-VL	NCO	286	8.1	0.4	450	0.3	30	50	15
	CO	329	8.2	0.0	450	0.2	30	40	0
	COH	165	7.2	0.2	310	−0.8	10	65	0

MAS NMR spectra did not affect the second-order line shape of the spectrum (Figure S6).[54]

The timing diagrams of the pulse sequences involving ^{17}O (3QMAS, MATPASS, ZF-TEDOR, REAPDOR, and R^3-R-INEPT) are illustrated in Figures S15 and S16 with the phase cycling scheme used for each experiment. The two-dimensional ^{17}O shifted-echo 3QMAS spectrum was acquired at 35.2 T with 20 rotor-synchronized t_1 increments with an increment of 52.63 μs, and performed with 3Q excitation and conversion pulses of 3 and 1 μs ($\gamma B_1/2\pi$ = 100 kHz), and $\pi/2$ and π pulses of 2.5 and 5 μs ($\gamma B_1/2\pi$ = 33.3 kHz). The two-dimensional ^{17}O magic-angle turning phase-adjusted sideband separation (MATPASS)[67] spectrum was acquired at 35.2 T with 8 t_1 increments with an increment of 26.3 μs and performed with $\pi/2$ and π pulses of 1.6 and 3.2 μs with $\gamma B_1/2\pi$ = 52 kHz. Two-dimensional ^{13}C−^{17}O ZF-TEDOR spectra were recorded at 21.1 T with 66 t_1 increments with an increment of 25 μs, a mixing time of 2.4 ms, and ^{13}C $\gamma B_1/2\pi$ = 100 kHz, ^{17}O $\gamma B_1/2\pi$ = 100 kHz and ^{1}H $\gamma B_1/2\pi$ = 100 kHz TPPM decoupling.[68] A series of one-dimensional ^{13}C−^{17}O ZF-TEDOR experiments with varying mixing times from 0.4 to 4.8 ms was performed to produce buildup curves. Two-dimensional ^{1}H−^{17}O R^3-R-INEPT[30,38,69] experiments were performed at 17.6 T with 40 t_1 increments with an increment of 25 μs, a R^3 pulse length of 100 μs at $\gamma B_1/2\pi$ = 20 kHz, and $\gamma B_1/2\pi$ = 100 kHz for hard pulses on ^{1}H and ^{17}O. One-dimensional ^{15}N−^{17}O ZF-TEDOR spectra were recorded at 17.6 T with ^{15}N $\gamma B_1/2\pi$ = 36 kHz, ^{17}O $\gamma B_1/2\pi$ = 100 kHz, and ^{1}H $\gamma B_1/2\pi$ = 100 kHz TPPM decoupling. Mixing times were varied from 2.33 to 20.09 ms to determine the maximum transfer. ^{15}N−^{17}O REAPDOR[36] was implemented at 17.6 T with dephasing times varying from 0.222 to 5.55 ms. The adiabatic ^{17}O pulse had a duration of one-third of a rotor period, $\tau_R/3$, and ^{17}O $\gamma B_1/2\pi$ = 100 kHz; the dipolar dephasing curve ($\Delta S/S$, where $\Delta S = S - S_R$) was determined by acquiring spectra with (S_R) and without (S) the ^{17}O adiabatic pulse.

^{13}C, ^{15}N cross-polarization (CP),[70,71] and ^{1}H MAS NMR experiments were performed at 11.7 T ($\omega_{0H}/2\pi$ = 500 MHz, home-built spectrometer courtesy of Dr. Dave Ruben, FBML-MIT) and 21.1 T, with $\omega_R/2\pi$ = 10 and 20 kHz, respectively. Two-dimensional ^{13}C−^{13}C (RFDR)[21] and ^{13}C−^{15}N (ZF-TEDOR)[72] experiments were performed at 11.7 T.

2.3. Spectral Processing and Simulations. All spectra were processed with RNMR (Dr. D. Ruben, FBML-MIT) or TOPSPIN (Bruker BioSpin, Billerica, MA, USA) with between 10 and 500 Hz of exponential apodization. Processing of the 3QMAS spectrum was done using home-written scripts in MATLAB (MathWorks Inc., Natick, MA, USA), which was necessary to Q-shear[73] the spectrum and "unwind" the spinning sidebands along the indirect dimension. Spectral simulations employed either the WSolids[74] or DMFit[75] software packages. The SIMPSON[76] and SPINEVOLUTION[77] software packages were used to simulate one-dimensional ^{15}N−^{17}O REAPDOR and ^{13}C−^{17}O ZF-TEDOR dephasing and buildups curves, respectively.

3. RESULTS AND DISCUSSION

3.1. ^{17}O Labeling of FMOC-Protected Amino Acids and N-Acetyl-L-valyl-L-leucine. To envisage ^{17}O NMR spectroscopy as a reliable tool for the study of biological solids, efficient enrichment of ^{17}O into biomolecules is paramount due to its low natural abundance (99.76% (^{16}O) vs 0.037% (^{17}O)). Recently, an efficient multiple-turnover labeling reaction has been described by Seyfried et al. that proceeds under mild conditions (i.e., room temperature and neutral pH) for ^{17}O/^{18}O enrichment of protected amino acids. The enrichment of various amino acids with different protecting groups was demonstrated by a reaction utilizing an excess of carbodiimide and H$_2$^{18}O with a dry proton source to eliminate racemization.[59]

Utilizing this multiple-turnover exchange reaction, FMOC-L-leucine and FMOC-L-valine were enriched with 40% ^{17}O-labeled H$_2$O (vide supra). The ^{17}O isotopic enrichment of the samples was determined by matrix-assisted laser desorption/ionization mass spectrometry (MALDI MS) (Koch Institute MIT), as shown in Figure S1. While the MALDI matrix appears at similar m/z to that of the FMOC amino acids (Figure S1a) these peaks did not interfere with the ability to determine the ^{17}O labeling of the samples. The MALDI MS results yielded the protected amino acids with a M$^+$ m/z of 376.4 Da for FMOC-L-leucine and 362.4 Da for FMOC-L-valine, the addition of a Na$^+$ ion to the molecule is the cause for the larger than expected m/z. For FMOC-L-leucine the mass spectra yielded peaks at m/z of 376.385, 377.383, and 378.420 Da corresponding to the M$^+$, (M+1)$^+$, and (M+2)$^+$, respectively. Correcting for the ^{13}C natural abundance yields a ^{16}O/^{16}O:^{16}O/^{17}O:^{17}O/^{17}O ratio of 36:38:26 for the FMOC-L-leucine sample, which corresponds to an ^{17}O enrichment of 45 ± 5%. The corrected ^{16}O/^{16}O:^{16}O/^{17}O:^{17}O/^{17}O ratio for the FMOC-L-valine sample was determined to be 37:42:20 that leads to an ^{17}O enrichment of 42 ± 5%. Therefore, the labeling efficiency of the multiple-turnover reaction for the two samples was determined to be 100% (40% ^{17}O, H$_2$^{17}O) within the error of measuring the enrichment. A new series of FMOC-[U-^{13}C,^{15}N]-L-leucine and FMOC-[U-^{13}C,^{15}N]-L-valine were then labeled with 70% ^{17}O-labeled H$_2$O for the synthesis of the dipeptide, N-acetyl-[U-^{13}C,^{15}N,70% ^{17}O]-L-valyl-L-leucine. N-Acetyl-[U-^{13}C,^{15}N,70% ^{17}O]-L-valyl-L-leucine was synthesized via solid-state peptide synthesis by New England Peptide (Gardner, MA), and the enrichment of ^{17}O was verified by MS (not shown) and ^{17}O MAS NMR (Figures 3 and S5).

3.2. 1D and 2D 3QMAS NMR of FMOC-Protected Amino Acids and N-Acetyl-L-valyl-L-leucine. The central transition of half-integer spin quadrupolar nucleus, such as ^{17}O (I = 5/2), is subject to residual second-order quadrupolar broadening under MAS that yields a characteristic line shape that can be used as a structural probe. The characteristic quadrupolar line shape can be described by the quadrupole coupling constant and the quadrupole asymmetry parameter, η_Q. In addition to the EFG tensor, the chemical shift tensor
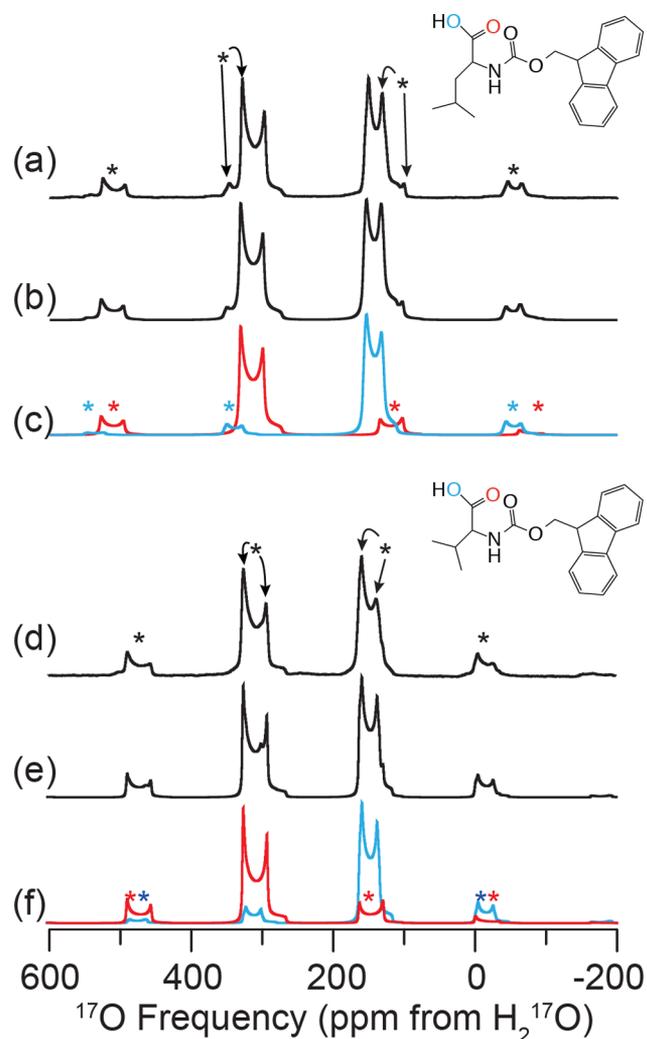
Figure 1. Experimental and simulated ^{17}O MAS NMR of FMOC-L-leucine (a−c) and FMOC-L-valine (d−f) at 21.1 T ($\omega_{0H}/2\pi$ = 900 MHz). Experimental ^{17}O MAS NMR (a,d), full spectral simulations (b,e), and simulations of each individual oxygen environment, CO (red) and COH (blue) (c,f) are shown. The line structures of FMOC-L-leucine (inset above (a)) and FMOC-L-valine (inset above (d)) indicating the oxygen environments of interest are displayed. Spectra were acquired with $\omega_R/2\pi$ = 24 (FMOC-L-leucine) or 20 (FMOC-L-valine) kHz, with spinning sidebands noted by asterisks (*). NMR parameters used in spectral simulations are given in Table 4.

Figure 2. Experimental ^{17}O MAS NMR of N-Ac-VL (a), full simulation of MAS NMR spectrum (b) and simulation of each individual oxygen environment (c) at 21.1 T ($\omega_{0H}/2\pi$ = 900 MHz). Line structure is shown in the inset indicating the ^{17}O enriched sites: CO (red), NCO (green) and COH (blue). Spectra were acquired with $\omega_R/2\pi$ = 24 kHz, spinning sidebands are noted by asterisks (*). NMR parameters used in spectral simulations are given in Table 4.

elements also influence the ^{17}O NMR spectrum, particularly at high fields due to the linear dependence of the chemical shift anisotropy (CSA) on the external magnetic field. The discussion that follows will employ the IUPAC definitions for chemical shift interactions adopting the Herzfeld−Berger convention.[66,78] The chemical shift tensor is described by the isotropic chemical shift, δ_{iso}, the breadth of the CSA powder pattern, span (Ω), and the magnitude of the asymmetry of the CSA tensor, skew (κ). More complete explanations of the EFG and CSA tensors in solids can be found in literature.[3,79−85]

^{17}O NMR at multiple magnetic fields (17.6−35.2 T) under both MAS and non-spinning conditions was utilized in conjunction with spectral simulations to determine the quadrupole and chemical shift tensor parameters for each oxygen site in the samples, as shown in Table 4, Figures 1−3, and Figures S3−S5.
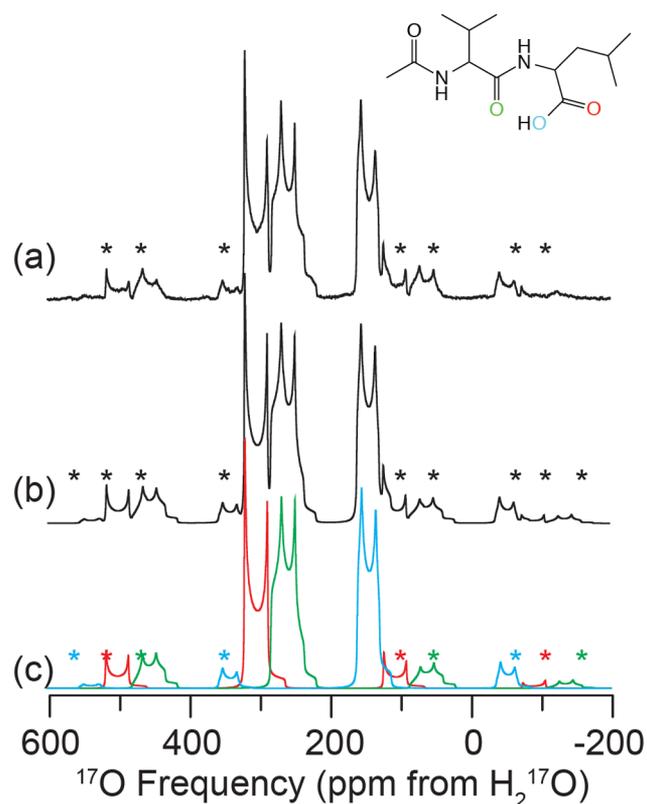
The MAS and non-spinning ^{17}O NMR spectra of FMOC-L-leucine are shown in Figures 1a−c and S4, and the ^{13}C−^{1}H CPMAS NMR spectrum is shown in Figure S2a. The ^{17}O C_Q of the CO and COH groups were found to be 8.3 and 7.3 MHz, respectively, with η_Q = 0.0 and 0.2. These values are consistent with previously reported studies of FMOC-protected amino acids.[10] The chemical shift parameters were found to be δ_{iso} = 338 and 161 ppm, Ω = 385 and 320 ppm, and κ = 0.1 and −0.8 for the CO and COH groups, respectively. FMOC-L-valine, as shown in Figures 1d−f and S4, was determined to have chemical shift tensor parameters, δ_{iso} = 337 and 169 ppm, Ω = 340 and 320 ppm, and κ = 0.2 and −0.7 for the CO and COH groups, respectively. The C_Q and η_Q were determined to be 8.45 and 7.45, and 0.0 and 0.15, respectively. Simulation of the chemical shift tensor parameters was necessary for both MAS and non-spinning spectra due to the large CSA of both oxygen environments and its effect on the intensities of the spinning sidebands present in the ^{17}O MAS spectra at 17.6 and 21.1 T.

Verification of a single crystalline structure of N-Ac-VL was achieved by performing one-dimensional ^{13}C, ^{15}N, and ^{1}H MAS NMR experiments, as shown in Figure S8, and comparing to previous studies.[18,72,86] Three crystallographically distinct oxygen environments were found within the structure of N-Ac-VL, one on the valine amino acid and two on the leucine, referred to as NCO, CO, and COH, respectively in the following discussion (as shown on the line structure in Figure 2). The ^{17}O NMR parameters of each ^{17}O site of N-Ac-VL were determined via ^{17}O MAS NMR at multiple magnetic
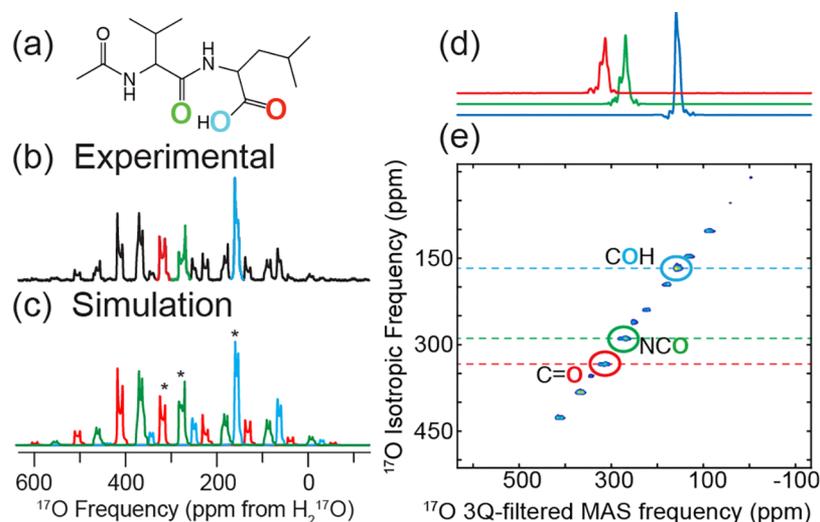
Figure 3. 1D and 2D ^{17}O MAS NMR spectra of [U-^{13}C,^{15}N,70% ^{17}O]-N-Ac-VL recorded at 35.2 T ($\omega_{0H}/2\pi$ = 1500 MHz). Line structure (a) of N-Ac-VL illustrating the positions labeled with ^{17}O (NCO, CO, and COH). Experimental (b) and simulated (c) 1D MAS ^{17}O MAS NMR spectra, spinning at 19 kHz; centerbands indicated with asterisks (*). Slices (d) of the anisotropic dimension of the 2D 3QMAS spectrum of N-Ac-VL extracted at the isotropic frequency of the centerbands of each ^{17}O moiety. (e) 2D 3QMAS spectrum of [U-^{13}C, ^{15}N, 70% ^{17}O]-N-Ac-VL at 35.2 T ($\omega_{0H}/2\pi$ = 1500 MHz) with the centerbands indicated with dashed horizontal lines and circles, the remaining peaks in the spectrum are due to spinning sidebands.

fields, as shown in Figures 2, 3 and S5. Spectral simulations were utilized to determine the quadrupole and chemical shift tensor parameters for each of the three ^{17}O sites (NCO, CO, and COH) in the sample, the results of which are summarized in Table 4. The C_Q was found to be 8.1, 8.2, and 7.2 for the NCO, CO, COH sites respectively, with η_Q of 0.4, 0.0, and 0.2. The chemical shift parameters of the NCO site were determined to be δ_{iso} = 286 ppm, Ω = 450 ppm and κ = 0.3. For the CO and COH sites these parameters were found to be δ_{iso} = 329 and 165, Ω = 450 and 310, and κ = 0.2 and −0.8, respectively (Table 4).

The relative uncertainty in the EFG tensor fits listed in Table 4 is primarily due to the inability to fully remove the spinning sidebands from the centerbands due to the large span of the second-order quadrupolar line shapes and the chemical shift dispersion in these samples. However, when spinning at $\omega_R/2\pi$ = 60 kHz, as shown in Figure S7 for FMOC-L-leucine and N-Ac-VL, the spinning sidebands no longer overlap with the centerband, and the C_Q and η_Q are fit with a higher degree of precision. While higher MAS frequencies result in a less ambiguous spectral simulation due to the attenuation of chemical shift tensor interaction and a fully resolved centerband spectrum; a loss of sample volume due to the reduced rotor size (i.e., 30 vs 2.5 μL) required for the increased spinning frequency results in a significant sacrifice in signal-to-noise and increase in acquisition time.

^{17}O MAS NMR experiments were performed at 35.2 T, as shown in Figures 3 and S14, to demonstrate the resolution that is afforded at high magnetic field strengths due to the inverse dependence of the second-order residual quadrupolar inter-action. Spectral simulation of the 1D MAS NMR spectrum verified the EFG and CSA tensors that were determined from different magnetic fields. The presence of intense spinning sidebands in the spectra recorded at 35.2 T is due to the spinning frequency that was employed ($\omega_R/2\pi$ = 19 kHz) and the increased influence of the CSA on the MAS NMR spectrum at the increased magnetic field. Therefore, the large effect of the CSA tensor on the line shape of each resonance, centerband

and spinning sidebands, increased the difficulty in producing an accurate spectral simulation. To isolate the contribution of the ^{17}O MAS NMR spectrum due to the spinning sidebands, 2D MATPASS was performed, as shown in Figure S14. The 2D MATPASS spectrum correlates the anisotropic spinning sideband order and the centerband only spectrum, thus allowing for more precise spectral simulation of the 1D MAS spectrum. To further demonstrate the resolution available at 35.2 T, 2D 3QMAS was performed (Figure 3d,e), yielding an isotropic dimension that does not suffer from the broad resonances of 1D MAS NMR experiments on quadrupolar nuclei. Extracting 1D slices at the isotropic frequency of each oxygen environment demonstrates the isolation of each of the environments and the triple-quantum filtered MAS line shape of the 2D resonances in the 3QMAS experiment (Figure 3d). The resolution that is produced by the two-dimensional 3QMAS experiment at high magnetic field will allow for complex samples to be probed via ^{17}O NMR spectroscopy.

3.3. ^{17}O Heteronuclear Correlation Experiments of N-Ac-VL Using Dipolar Recoupling Methods. Early studies to validate the use of heteronuclear correlation experiments to measure dipolar couplings in spin I = 1/2 nuclei were performed on small peptides, including N-Ac-VL.[18,72,87,88] Jaroniec et al. utilized one-dimensional and two-dimensional heteronuclear correlation experiments to measure ^{13}C−^{15}N dipolar couplings in N-Ac-VL via frequency-selective REDOR, while using RFDR and ZF-TEDOR for resonance assign-ments.[18,72] To further validate the ^{17}O-enriched N-Ac-VL sample used here, two-dimensional ^{13}C−^{13}C RFDR and ^{13}C−^{15}N ZF-TEDOR were performed (Figures S9 and S10) and compared to the previous results.

Two-dimensional MAS NMR correlation spectroscopy of half-integer quadrupolar nuclei, like ^{17}O, has yet to be utilized routinely for biologically relevant samples.[10] However, one-dimensional dephasing experiments such as REAPDOR, TRAPDOR, and REDOR have been shown to measure isolated spin pairs in biological samples, though these experiments require a well resolved one-dimensional spectra and a simple

Table 5. O–C/N/H Intra- and Intermolecular Distances of Interest within N-Ac-VL

O	C/N/H	r_{cryst} (Å)[a]	D (Hz)[a]	r_{NMR} (Å)[b]	experiment	description
			Intramolecular N-Ac-VL Contacts			
O2	C3	2.414	291.3	$2.5_0 \pm 0.1_5$	TEDOR	NCO-Vα
	C7	1.231	2196.4	$1.2_3 \pm 0.1_5$	TEDOR	NCO-V'
	C8	2.681	212.6	$2.7_3 \pm 0.1_5$	TEDOR	NCO-Lα
	N1	2.784	76.5	$2.9_3 \pm 0.2$	REAPDOR	NCO-N$_V$
	N2	2.226	149.8	$2.3_6 \pm 0.2$	REAPDOR	NCO-N$_L$
O3	C8	2.375	305.4	$2.4_2 \pm 0.1_5$	TEDOR	CO-Lα
	C13	1.196	2394.9	$1.2_5 \pm 0.1_5$	TEDOR	CO-L'
O4	C8	2.384	302.4	$2.4_3 \pm 0.1_5$	TEDOR	COH-Lα
	C13	1.308	1830.9	$1.4_5 \pm 0.1_5$	TEDOR	COH-L'
	N2	2.749	79.5	3.0 ± 0.2	REAPDOR	COH-N$_L$
	H24	0.859	25701.9	–	R^3-R-INEPT	COH-H$_{L'}$
			Intermolecular N-Ac-VL Contacts			
O2	H24	1.784	2869.2	-	R^3-R-INEPT	NCO-H$_{L'}$
O3	N1	2.884	68.86	$3.2_1 \pm 0.2$	REAPDOR	CO-N$_V$
	H22	1.967	2140.6	-	R^3-R-INEPT	CO-H$_{Nv}$

[a]Distances and couplings taken from ref 92. [b]Current study.

spin system to simulate.[10,45,89−91] Despite these limitations, utilizing specific labeling techniques Dupree and co-workers were able to measure $^{15}N-^{17}O$ interatomic distances in two amyloid-beta peptides using $^{15}N-^{17}O$ REAPDOR.[4,37] Including ^{17}O as a routine nucleus of interest in NMR structural studies of biological systems requires augmenting the known one-dimensional techniques for measuring spin $I = 1/2$ to ^{17}O distances with the better resolved two-dimensional qualitative and quantitative correlation experiments used for spin $I = 1/2$ nuclei.

Dipolar dephasing and recoupling experiments of N-Ac-VL were examined to further investigate both the crystal structure of N-Ac-VL and the viability of such techniques for further biological structure studies. Interatomic distances were determined via SIMPSON[76] and SPINEVOLUTION[77] simulations based on one-dimensional $^{15}N-^{17}O$ REAPDOR dephasing curves and $^{13}C-^{17}O$ ZF-TEDOR buildup curves, and are given in Table 5. $^{15}N-^{17}O$ REAPDOR experiments probed the $^{15}N-^{17}O$ dipolar couplings in the crystal, as shown in Figure 4. While the REAPDOR results demonstrate the robustness of dipolar dephasing experiments to measure accurate distances involving ^{17}O, to properly fit each dephasing curve the simulation required two ^{17}O nuclei for each ^{15}N resonance. Dipolar dephasing experiments yield accurate measurements of the dipolar coupling between isolated spin pairs; however, when an isolated two-spin system is not present the resulting simulations require multiple dipolar couplings and therefore reducing the accuracy of the resulting distance measurement due to the increase in variables. Despite this limitation, the $^{15}N-^{17}O$ distances extracted from the simulated dephasing curves were within 12%[29] of the distances determined via X-ray diffraction methods.[92] The $^{15}N-^{17}O$ distances extracted from the leucine nitrogen (L$_N$) dephasing curve were found to be 2.36 Å to the NCO oxygen and 3.0 Å to the COH oxygen compared to 2.226 and 2.749 Å from diffraction. Weaker dipolar couplings were not included in the simulations to limit the size of the spin system and the number of matrix variables; however, inclusion of a larger number of
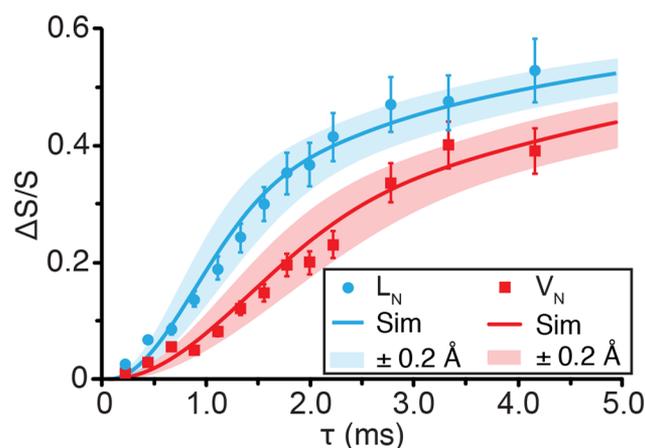

Figure 4. One-dimensional $^{15}N-^{17}O$ REAPDOR dephasing curves of the leucine (blue, circle) and valine (red, squares) nitrogens of N-Ac-VL at 17.6 T ($\omega_{0H}/2\pi$ = 750 MHz). Best-fit simulated REAPDOR dephasing curves (solid lines) and ± 0.2 Å error (semi-transparent curve) in simulated dephasing curves generated using SIMPSON.[76] $^{15}N-^{17}O$ distances that were determined based on the simulated curves are given in Table 5.

dipolar couplings could yield a more accurate distance measurement. This limitation of REAPDOR can be avoided by using either a sample that is specifically labeled to isolate the spin pairs of interest or via a correlation experiment that utilizes a second dimension to increase the resolution of the experiment. The 1D $^{15}N-^{17}O$ ZF-TEDOR spectrum, as shown in Figure S11, demonstrated the ability to utilize ZF-TEDOR to transfer polarization from ^{15}N to ^{17}O nuclei in biological solids. However, the sensitivity of the experiment prevented $^{15}N-^{17}O$ distances from being measured via a one-dimensional buildup or a full two-dimensional experiment, an area that dynamic nuclear polarization (DNP) will surely impact.

$^{13}C-^{17}O$ ZF-TEDOR was performed, as shown in Figures 5 and 6, to further probe the ^{17}O interatomic distances in the N-
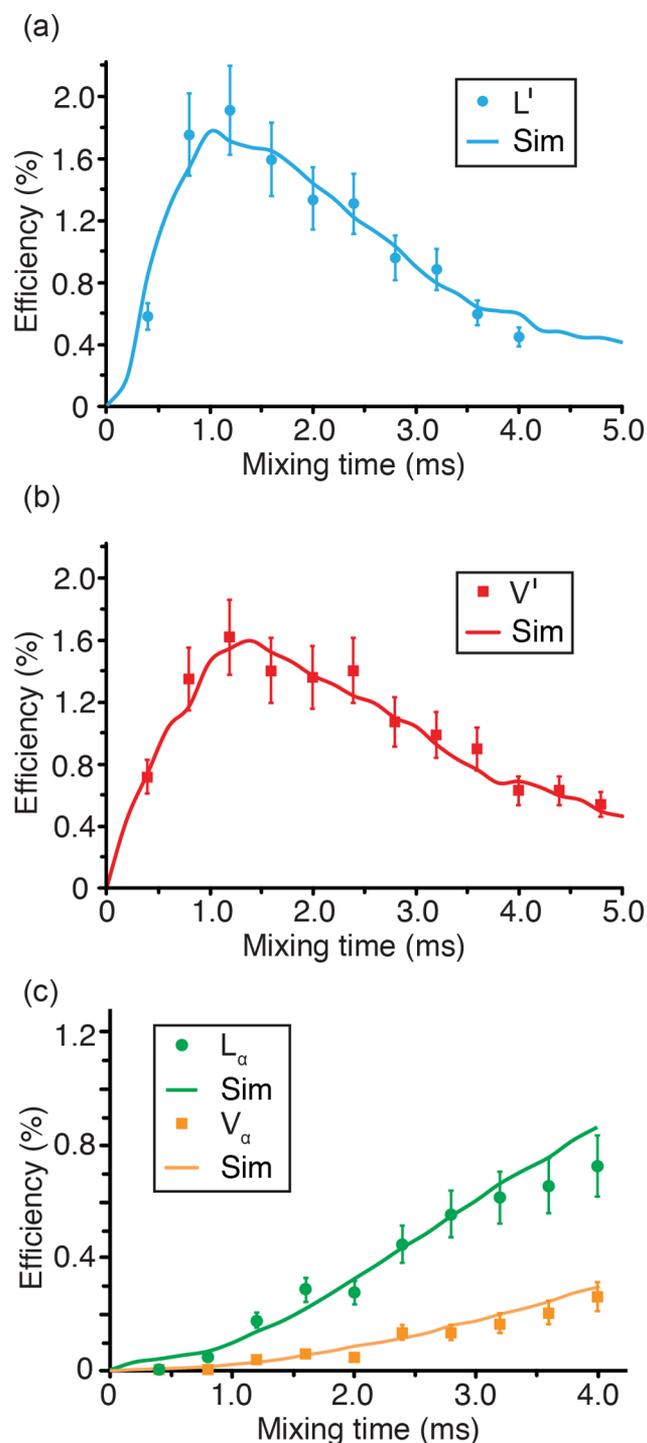
(a)

(b)

(c)

Figure 5. Experimental and simulated one-dimensional $^{13}C-^{17}O$ ZF-TEDOR buildup curves as a function of mixing for the leucine carbonyl (a), valine carbonyl (b), and $C\alpha$ (c) sites (leucine, green circles and valine, orange squares) at 21.1 T ($\omega_{0H}/2\pi$ = 900 MHz) with $\gamma B_1/2\pi$ (^{17}O) = 100 kHz, and 100 kHz TPPM ^1H decoupling during acquisition. Best fit simulated curves (solid lines) determined using SPINEVOLUTION.[77] $^{13}C-^{17}O$ distances that were determined based on the simulated curves are given in Table 5.

Figure 6. Two-dimensional $^{13}C-^{17}O$ ZF-TEDOR spectrum recorded at 21.1 T ($\omega_{0H}/2\pi$ = 900 MHz) with 2.4 ms of mixing. Correlations between the NCO and CO oxygen sites with the closest C′ and Cα indicated on the line structure of N-Ac-VL in the inset.

Ac-VL crystal structure. The combination of the higher sensitivity of ^{13}C detection with the increase in magnetic field strength (21.1 vs 17.6 T) allowed for both one-dimensional buildup curves and a two-dimensional correlation spectrum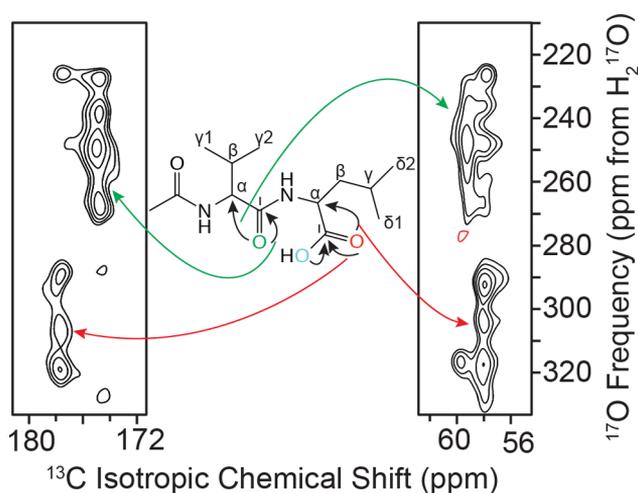 to be collected for the N-Ac-VL sample. The one-dimensional buildup curves, performed with mixing times from 0.4 to 4.8 ms, allowed for $^{13}C-^{17}O$ interatomic distances to be determined via simulation of the curves, as given in Table 5. Due to the insensitivity of the ZF-TEDOR experiment, the buildup curves were not performed by determining the cross peak intensity as a function of mixing time from multiple two-dimensional TEDOR experiments. The $^{13}C-^{17}O$ distances determined by the fitting of the $^{13}C-^{17}O$ ZF-TEDOR curves were within 10% of those determined by diffraction methods.[92] For the ZF-TEDOR experiments, $^{13}C-^{17}O$ distances could be probed for both the carbonyl and the alpha carbons of the sample, demonstrating an increase in the number of ^{17}O contacts that can be probed via $^{13}C-^{17}O$ ZF-TEDOR when compared to $^{15}N-^{17}O$ REAPDOR. The dependence of the ZF-TEDOR experiment is sensitive to the orientation of the quadrupolar interaction relative to the internuclear vector rendering the simulations of the curves quite sensitive to the atomic-level molecular structure. While it is difficult to precisely measure the orientation of the quadrupolar tensor with respect to the internuclear vector, extraction of the Euler angles between the EFG and CSA tensors were possible by spectral simulations of the 1D ^{17}O MAS NMR spectra of N-Ac-VL, as given in Table 4. These angles were then used for the simulation of the ZF-TEDOR buildup curves to reduce the number of variables within the simulation. Narrowing of the possible orientations of the ^{17}O quadrupolar interaction allowed for the ZF-TEDOR simulations to be completed within an experimental error of ±0.15 Å, as shown in Figure 5. The ZF-TEDOR buildup curves of the carbonyl resonances (V′ and L′) were fit to one and two $^{13}C-^{17}O$ distances respectively for the valine and leucine peaks. These fits were determined by iteratively simulating the buildup curves starting with the $^{13}C-^{17}O$ distances from the previously determined crystal structure.[92] The distances that were extracted from these fits were found to be 1.23 Å for V′-NCO, 1.25 Å for L′-CO, and 1.45 Å for L′-COH; these $^{13}C-^{17}O$ distances are slightly longer than the diffraction values of 1.23, 1.196, and 1.308 Å. The Cα resonances were simulated using one and three $^{13}C-^{17}O$ distances for each ^{13}C resonance. The Cα simulations yielded $^{13}C-^{17}O$ distances of 2.50 Å for Vα-NCO, 2.42 Å for Lα-CO, 2.43 Å for Lα-COH, and 2.73 Å for Lα-NCO. The $^{13}C-^{17}O$

distances extracted from the simulations of the ZF-TEDOR experiments were determined to be within 0.15 Å of those determined by diffraction,[92] which is within the error present in ^{13}C−^{15}N TEDOR measurements on N-Ac-VL.[72] The ^{13}C−^{17}O distances were measured to be slightly longer than the distances determined by X-ray diffraction, which could be due to the fact that additional couplings could be contributing to the buildup curves that were not included in the simulations due to the size of the nuclear spin system. Figure S12 shows the ZF-TEDOR buildup curves with not only the best-fit simulation but also the ±0.15 Å error for each curve, indicating the precision of the simulation method. The ZF-TEDOR simulations show a much larger dependence on the crystallite orientation and thus required a total of 5,702,887 crystal angle combinations to achieve the curves shown in Figures 5 and S12. Simulations with a smaller set of crystallite orientations yielded curves with more pronounced and non-uniform modulations convoluted with the proper dipolar coupling-dependent curve.

Two-dimensional ^{13}C−^{17}O ZF-TEDOR was performed, as shown in Figure 5, demonstrating the resolution that is available to the ZF-TEDOR experiment. The two-dimensional ZF-TEDOR spectra was collected over the course of 4 days with a mixing time of 2.4 ms, which corresponds to a transfer efficiency of ∼1.4 and 0.4% for the carbonyl and alpha carbons. The L′ and Lα correlations to COH are not shown in Figure 5 due to the low intensity of these peaks that likely arises from the imprecise nature of the π pulses on this particular ^{17}O resonance (π pulses for the two-dimensional ZF-TEDOR spectra were calibrated on the NCO resonance). The differing C_Q value for the COH oxygen in comparison to the NCO and CO oxygens causes the COH oxygen to have a slightly altered nutation frequency in comparison to the other oxygens. However, the one-dimensional ZF-TEDOR buildup curves required the addition of the COH dipolar coupling and orientation to properly match the experimental shape indicating that magnetization transfer to the COH environment is occurring. As is evident in Figure 6, the two-dimensional ZF-TEDOR spectrum suffers from a lack of sensitivity that is apparent in the low signal-to-noise of the spectrum despite the long acquisition time. Despite the low signal-to-noise, the cross peaks within the spectrum demonstrate the ability of ^{17}O NMR to act as a powerful probe of interactions between ^{13}C and ^{17}O spins within biomolecular solids. While in the current study ^{13}C−^{17}O interactions were limited to couplings equivalent to one- and two-bond distances, with an increased sensitivity the ZF-TEDOR experiment could be extended to a larger range of carbon−oxygen interactions.

To directly examine hydrogen bonding within the N-Ac-VL crystal, ^{1}H−^{17}O correlation spectroscopy was performed via the ^{1}H detected R^3-R-INEPT experiment. The use of ^{1}H detection takes advantage of the higher sensitivity and narrower line widths of ^{1}H in comparison to ^{17}O in addition to utilizing the fast relaxation of the quadrupolar nucleus allowing for rapid recycling of the experiment and thus shorter experimental times. The one-dimensional and two-dimensional ^{1}H−^{17}O R^3-R-INEPT spectra, as shown in Figure 7, show the correlation of the COH ^{1}H (H$_{L'}$) to the COH and NCO oxygens. While the expected directly bonded oxygen is seen in this experiment, the more significant finding is the intermolecular correlation between the carbonyl proton and the NCO oxygen. A low signal-to-noise peak for the H$_{L'}$−CO correlation was seen in a two-dimensional R^3-R-INEPT experiment using an R^3 pulse
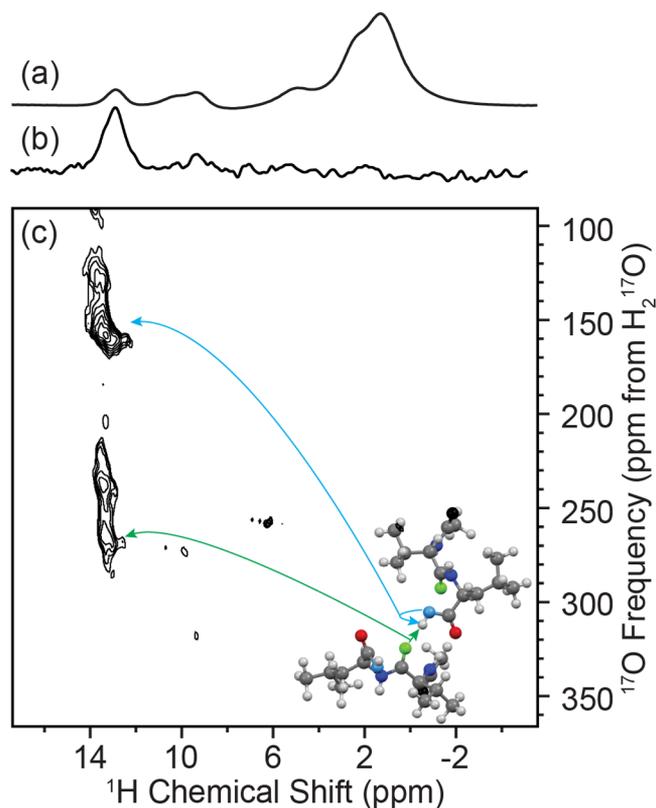

Figure 7. MAS NMR spectroscopy of N-Ac-VL: (a) ^{1}H direct Hahn-echo detection, (b) one-dimensional ^{1}H−^{17}O R^3-R-INEPT, (c) and two-dimensional ^{1}H−^{17}O R^3-R-INEPT spectrum with R^3 = 100 μs. Spectra were acquired with $\omega_R/2\pi$ = 20 kHz at 17.6 T ($\omega_{0H}/2\pi$ = 750 MHz). Correlations between the leucine carbonyl proton to its directly bonded oxygen (blue arrow) and its next closest oxygen through space (NCO, green arrow) are indicated on the crystal structure of N-Ac-VL in the inset.[92]

length of 100 μs (Figure S13). The two-dimensional ^{1}H-detected ^{17}O correlation experiment demonstrates the ability to directly probe hydrogen bonding, demonstrating the intermolecular contact between the leucine and valine residues of adjacent N-Ac-VL.

4. CONCLUSIONS

An efficient multiple-turnover reaction for ^{17}O enrichment was used to ^{17}O enrich two FMOC-protected amino acids, L-leucine and L-valine, which were used as precursors for the synthesis of a uniformly ^{13}C,^{15}N-labeled and 70% ^{17}O-labeled dipeptide, N-Ac-VL. The ^{17}O quadrupolar and chemical shift parameters for the FMOC-protected amino acid precursors and the dipeptide were determined using multiple magnetic fields and spinning frequencies. The EFG tensor parameters for the FMOC-protected amino acids were found to be similar for each of the two oxygen environments, C_Q = 8.4 and 7.3 MHz and η_Q = 0 and 0.2. The leucine residue of the N-Ac-VL was found to have similar quadrupolar and chemical shift parameters to the FMOC-L-leucine sample. However, the oxygen environment of the valine residue was found to have a C_Q and η_Q similar to other peptide NCO environments (8.4 MHz and 0.4). ^{17}O NMR experiments were performed at 35.2 T to demonstrate the ability of high magnetic fields to increase the sensitivity and resolution of ^{17}O MAS NMR spectra via 1D (MAS) and 2D (MATPASS and 3QMAS) experiments. One- and two-

dimensional correlation experiments between ^{17}O and $^{15}N/^{13}C/^{1}H$ using dipolar recoupling methods were performed on N-Ac-[U-^{13}C,^{15}N,70% ^{17}O]-VL demonstrating the viability of ^{17}O NMR as a tool for structural studies of biological systems. $^{15}N-^{17}O$ and $^{13}C-^{17}O$ interatomic distances were directly measured via dephasing and buildup curves of REAPDOR and ZF-TEDOR experiments and determined to be within 15% of previously reported values. The two-dimensional ^{17}O correlation spectra showed the ability to measure ^{17}O connectivity within a dipeptide and demonstrated the ability to utilize the increased resolution of two-dimensional experiments to study more complex systems in the future. ^{1}H detected ^{17}O NMR was used to directly probe through space hydrogen bonding in the dipeptide; showing the ability to use ^{17}O NMR to directly measure connectivity via hydrogen bonding. The addition of multiple-quantum filters and DNP NMR would allow for the ^{17}O correlation experiments to be performed with reduced experiment times and increased spectral resolution. Thus, enabling ZF-TEDOR buildup curves to be produced from the cross peak intensities of multiple two-dimensional experiments, and for a larger range of mixing times to probe weaker $^{13}C-^{17}O$ dipolar couplings that were not observed in the one-dimensional ZF-TEDOR buildups. With the enhanced signal-to-noise the R^3-R-INEPT experiment could be extended to probe $^{1}H-^{17}O$ interatomic distances similarly to ZF-TEDOR.

ASSOCIATED CONTENT

Ⓢ Supporting Information

The Supporting Information is available free of charge on the ACS Publications website at DOI: 10.1021/jacs.7b08989.

Additional Figures S1–S16, showing spectra, buildup curves, and pulse sequences (PDF)

AUTHOR INFORMATION

Corresponding Author

*rgg@mit.edu

ORCID Ⓘ

Eric G. Keeler: 0000-0002-9598-7148

Robert G. Griffin: 0000-0003-1589-832X

Present Addresses

§E.G.K.: Department of Chemistry, Columbia University, New York, NY 10027, USA

⊥V.K.M.: Department of Chemistry, University of Alberta, Edmonton, Alberta T6G 2G2, Canada

∥M.T.C.: Ortho Clinical Diagnostics, Rochester, NY 14626, USA

Notes

The authors declare no competing financial interest.

ACKNOWLEDGMENTS

REFERENCES

(1) Glowacki, E. D.; Irimia-Vladu, M.; Bauer, S.; Sariciftci, N. S. *J. Mater. Chem. B* **2013**, *1*, 3742−3753.

(2) Horowitz, S.; Trievel, R. C. *J. Biol. Chem.* **2012**, *287*, 41576−41582.

(3) Grandinetti, P. J.; Trease, N. M.; Ash, J. T. *Prog. Nucl. Magn. Reson. Spectrosc.* **2011**, *59*, 121−196.

(4) Antzutkin, O. N.; Iuga, D.; Filippov, A. V.; Kelly, R. T.; Becker-Baldus, J.; Brown, S. P.; Dupree, R. *Angew. Chem., Int. Ed.* **2012**, *51*, 10289−10292.

(5) Aguiar, P. M.; Michaelis, V. K.; McKinley, C. M.; Kroeker, S. *J. Non-Cryst. Solids* **2013**, *363*, 50−56.

(6) Kong, X.; Shan, M.; Terskikh, V.; Hung, I.; Gan, Z.; Wu, G. *J. Phys. Chem. B* **2013**, *117*, 9643−9654.

(7) Kwan, I.; Mo, X.; Wu, G. *J. Am. Chem. Soc.* **2007**, *129*, 2398−2407.

(8) Zhu, J.; Ye, E.; Terskikh, V.; Wu, G. *Angew. Chem., Int. Ed.* **2010**, *49*, 8399−8402.

(9) Michaelis, V. K.; Keeler, E. G.; Ong, T.-C.; Craigen, K. N.; Penzel, S. A.; Wren, J. E. C.; Kroeker, S.; Griffin, R. G. *J. Phys. Chem. B* **2015**, *119*, 8024−36.

(10) Wong, A.; Poli, F. *Annu. Rep. NMR Spectrosc.* **2014**, *83*, 145−220.

(11) Wu, G. *Solid State Nucl. Magn. Reson.* **2016**, *73*, 1−14.

(12) Kong, X. Q.; Brinkmann, A.; Terskikh, V.; Wasylishen, R. E.; Bernard, G. M.; Duan, Z.; Wu, Q. C.; Wu, G. *J. Phys. Chem. B* **2016**, *120*, 11692−11704.

(13) Tang, A. W.; Kong, X. Q.; Terskikh, V.; Wu, G. *J. Phys. Chem. B* **2016**, *120*, 11142−11150.

(14) Chekmenev, E. Y.; Waddell, K. W.; Hu, J.; Gan, Z. H.; Wittebort, R. J.; Cross, T. A. *J. Am. Chem. Soc.* **2006**, *128*, 9849−9855.

(15) Waddell, K. W.; Chekmenev, E. Y.; Wittebort, R. J. *J. Phys. Chem. B* **2006**, *110*, 22935−22941.

(16) Zhang, Q. W.; Chekmenev, E. Y.; Wittebort, R. J. *J. Am. Chem. Soc.* **2003**, *125*, 9140−9146.

(17) Griffin, R. G. *Nat. Struct. Biol.* **1998**, *5*, 508−512.

(18) Jaroniec, C. P.; Tounge, B. A.; Herzfeld, J.; Griffin, R. G. *J. Am. Chem. Soc.* **2001**, *123*, 3507−3519.

(19) McDowell, L. M.; Schaefer, J. *Curr. Opin. Struct. Biol.* **1996**, *6*, 624−629.

(20) Opella, S. J. *Nat. Struct. Biol.* **1997**, *4*, 845−848.

(21) Bennett, A. E.; Ok, J. H.; Griffin, R. G.; Vega, S. *J. Chem. Phys.* **1992**, *96*, 8624−8627.

(22) De Paepe, G.; Lewandowski, J. R.; Loquet, A.; Eddy, M.; Megy, S.; Bockmann, A.; Griffin, R. G. *J. Chem. Phys.* **2011**, *134*, 095101.

(23) De Paepe, G.; Lewandowski, J. R.; Loquet, A.; Bockmann, A.; Griffin, R. G. *J. Chem. Phys.* **2008**, *129*, 245101.

(24) Gullion, T.; Schaefer, J. *J. Magn. Reson.* **1989**, *81*, 196−200.

(25) Hing, A. W.; Vega, S.; Schaefer, J. *J. Magn. Reson.* **1992**, *96*, 205−209.

(26) Munowitz, M. G.; Griffin, R. G.; Bodenhausen, G.; Huang, T. H. *J. Am. Chem. Soc.* **1981**, *103*, 2529−2533.

(27) Munowitz, M. G.; Griffin, R. G. *J. Chem. Phys.* **1982**, *76*, 2848−2858.

(28) Roberts, J. E.; Harbison, G. S.; Munowitz, M. G.; Herzfeld, J.; Griffin, R. G. *J. Am. Chem. Soc.* **1987**, *109*, 4163−4169.

(29) Hung, I.; Uldry, A. C.; Becker-Baldus, J.; Webber, A. L.; Wong, A.; Smith, M. E.; Joyce, S. A.; Yates, J. R.; Pickard, C. J.; Dupree, R.; et al. *J. Am. Chem. Soc.* **2009**, *131*, 1820−1834.

(30) Trebosc, J.; Hu, B.; Amoureux, J. P.; Gan, Z. *J. Magn. Reson.* **2007**, *186*, 220−227.

(31) Perras, F. A.; Chaudhary, U.; Slowing, I. I.; Pruski, M. *J. Phys. Chem. C* **2016**, *120*, 11535−11544.

(32) Perras, F. A.; Kobayashi, T.; Pruski, M. *J. Am. Chem. Soc.* **2015**, *137*, 8336−8339.

(33) Michaelis, V. K.; Markhasin, E.; Daviso, E.; Herzfeld, J.; Griffin, R. G. *J. Phys. Chem. Lett.* **2012**, *3*, 2030−2034.

(34) Vogt, F. G.; Yin, H.; Forcino, R. G.; Wu, L. M. *Mol. Pharmaceutics* **2013**, *10*, 3433−3446.

(35) Amoureux, J. P.; Trebosc, J.; Tricot, G. *Magn. Reson. Chem.* **2007**, *45*, S187−S191.

(36) Gullion, T. *Chem. Phys. Lett.* **1995**, *246*, 325−330.

(37) Wei, J.; Antzutkin, O. N.; Filippov, A. V.; Iuga, D.; Lam, P. Y.; Barrow, M. P.; Dupree, R.; Brown, S. P.; O'Connor, P. B. *Biochemistry* **2016**, *55*, 2065−2068.

(38) Martineau, C.; Bouchevreau, B.; Taulelle, F.; Trebosc, J.; Lafon, O.; Amoureux, J. P. *Phys. Chem. Chem. Phys.* **2012**, *14*, 7112−7119.

(39) Brinkmann, A.; Kentgens, A. P. M. *J. Am. Chem. Soc.* **2006**, *128*, 14758−14759.

(40) Prasad, S.; Clark, T. M.; Sharma, R.; Kwak, H.-T.; Grandinetti, P. J.; Zimmermann, H. *Solid State Nucl. Magn. Reson.* **2006**, *29*, 119−124.

(41) Prasad, S.; Kwak, H. T.; Clark, T.; Grandinetti, P. J. *J. Am. Chem. Soc.* **2002**, *124*, 4964−4965.

(42) Blanc, F.; Sperrin, L.; Jefferson, D. A.; Pawsey, S.; Rosay, M.; Grey, C. P. *J. Am. Chem. Soc.* **2013**, *135*, 2975−2978.

(43) Michaelis, V. K.; Corzilius, B.; Smith, A. A.; Griffin, R. G. *J. Phys. Chem. B* **2013**, *117*, 14894−14906.

(44) Michaelis, V. K.; Ong, T. C.; Kiesewetter, M. K.; Frantz, D. K.; Walish, J. J.; Ravera, E.; Luchinat, C.; Swager, T. M.; Griffin, R. G. *Isr. J. Chem.* **2014**, *54*, 207−221.

(45) Gullion, T.; Yamauchi, K.; Okonogi, M.; Asakura, T. *Macromolecules* **2007**, *40*, 1363−1365.

(46) Yamada, K.; Yamazaki, T.; Asanuma, M.; Hirota, H.; Yamamoto, N.; Kajihara, Y. *Chem. Lett.* **2007**, *36*, 192−193.

(47) Sefzik, T. H.; Houseknecht, J. B.; Clark, T. M.; Prasad, S.; Lowary, T. L.; Gan, Z.; Grandinetti, P. J. *Chem. Phys. Lett.* **2007**, *434*, 312−315.

(48) Wong, A.; Beevers, A. J.; Kukol, A.; Dupree, R.; Smith, M. E. *Solid State Nucl. Magn. Reson.* **2008**, *33*, 72.

(49) Wong, A.; Howes, A. P.; Yates, J. R.; Watts, A.; Anupold, T.; Past, J.; Samoson, A.; Dupree, R.; Smith, M. E. *Phys. Chem. Chem. Phys.* **2011**, *13*, 12213−12224.

(50) Wu, G.; Dong, S.; Ida, R.; Reen, N. *J. Am. Chem. Soc.* **2002**, *124*, 1768.

(51) Yamauchi, K.; Okonogi, M.; Kurosu, H.; Tansho, M.; Shimizu, T.; Gullion, T.; Asakura, T. *J. Magn. Reson.* **2008**, *190*, 327.

(52) Zhu, J.; Lau, J. Y. C.; Wu, G. *J. Phys. Chem. B* **2010**, *114*, 11681−11688.

(53) Wu, G. Oxygen 17 NMR Studies of Organic and Biological Molecules. In *eMagRes*, John Wiley & Sons, Ltd.: Chichester, UK; 2011 (DOI: 10.1002/9780470034590.emrstm1212).

(54) Keeler, E. G.; Michaelis, V. K.; Griffin, R. G. *J. Phys. Chem. B* **2016**, *120*, 7851−7858.

(55) Lemaitre, V.; Pike, K. J.; Watts, A.; Anupold, T.; Samoson, A.; Smith, M. E.; Dupree, R. *Chem. Phys. Lett.* **2003**, *371*, 91−97.

(56) Pike, K. J.; Lemaitre, V.; Kukol, A.; Anupold, T.; Samoson, A.; Howes, A. P.; Watts, A.; Smith, M. E.; Dupree, R. *J. Phys. Chem. B* **2004**, *108*, 9256−9263.

(57) Wong, A.; Howes, A. P.; Pike, K. J.; Lemaitre, V.; Watts, A.; Anupold, T.; Past, J.; Samoson, A.; Dupree, R.; Smith, M. E. *J. Am. Chem. Soc.* **2006**, *128*, 7744−7745.

(58) O'Dell, L. A.; Ratcliffe, C. I.; Kong, X.; Wu, G. *J. Phys. Chem. A* **2012**, *116*, 1008−1014.

(59) Seyfried, M. S.; Lauber, B. S.; Luedtke, N. W. *Org. Lett.* **2010**, *12*, 104−106.

(60) Mijalis, A. J.; Thomas, D. A., 3rd; Simon, M. D.; Adamo, A.; Beaumont, R.; Jensen, K. F.; Pentelute, B. L. *Nat. Chem. Biol.* **2017**, *13*, 464−466.

(61) Etzkorn, M.; Raschle, T.; Hagn, F.; Gelev, V.; Rice, A. J.; Walz, T.; Wagner, G. *Structure* **2013**, *21*, 394−401.

(62) Marecek, J.; Song, B.; Brewer, S.; Belyea, J.; Dyer, R. B.; Raleigh, D. P. *Org. Lett.* **2007**, *9*, 4935−4937.

(63) Steinschneider, A.; Burgar, M. I.; Buku, A.; Fiat, D. *Int. J. Pept. Protein Res.* **1981**, *18*, 324−333.

(64) Theodorou, V.; Skobridis, K.; Alivertis, D.; Gerothanassis, I. P. *J. Labelled Compd. Radiopharm.* **2014**, *57*, 481−508.

(65) Gan, Z.; Hung, I.; Wang, X.; Paulino, J.; Wu, G.; Litvak, I. M.; Gor'kov, P. L.; Brey, W. W.; Lendi, P.; Schiano, J. L.; et al. *J. Magn. Reson.* **2017**, *284*, 125.

(66) Harris, R. K.; Becker, E. D.; De Menezes, S. M. C.; Granger, P.; Hoffman, R. E.; Zilm, K. W. *Pure Appl. Chem.* **2008**, *80*, 59−84.

(67) Hung, I.; Gan, Z. H. *J. Magn. Reson.* **2010**, *204*, 150−154.

(68) Bennett, A. E.; Rienstra, C. M.; Auger, M.; Lakshmi, K. V.; Griffin, R. G. *J. Chem. Phys.* **1995**, *103*, 6951−6958.

(69) Morris, G. A.; Freeman, R. *J. Am. Chem. Soc.* **1979**, *101*, 760−762.

(70) Schaefer, J.; Stejskal, E. O. *J. Am. Chem. Soc.* **1976**, *98*, 1031−1032.

(71) Pines, A.; Waugh, J. S.; Gibby, M. G. *J. Chem. Phys.* **1972**, *56*, 1776−1777.

(72) Jaroniec, C. P.; Filip, C.; Griffin, R. G. *J. Am. Chem. Soc.* **2002**, *124*, 10728−10742.

(73) Hung, I.; Trebosc, J.; Hoatson, G. L.; Vold, R. L.; Amoureux, J. P.; Gan, Z. H. *J. Magn. Reson.* **2009**, *201*, 81−86.

(74) Eichele, K. *WSolids1 NMR Simulation Package*, 1.20.21; 2013.

(75) Massiot, D.; Fayon, F.; Capron, M.; King, I.; Le Calve, S.; Alonso, B.; Durand, J. O.; Bujoli, B.; Gan, Z. H.; Hoatson, G. *Magn. Reson. Chem.* **2002**, *40*, 70−76.

(76) Bak, M.; Rasmussen, J. T.; Nielsen, N. C. *J. Magn. Reson.* **2000**, *147*, 296−330.

(77) Veshtort, M.; Griffin, R. G. *J. Magn. Reson.* **2006**, *178*, 248−282.

(78) Herzfeld, J.; Berger, A. E. *J. Chem. Phys.* **1980**, *73*, 6021−6030.

(79) Ashbrook, S. E.; Smith, M. E. *Chem. Soc. Rev.* **2006**, *35*, 718−735.

(80) Man, P. P. *Encyclopedia of Analytical Chemistry*; John Wiley and Sons: Chichester, 2000; pp 12224−12265.

(81) Saito, H.; Ando, I.; Ramamoorthy, A. *Prog. Nucl. Magn. Reson. Spectrosc.* **2010**, *57*, 181−228.

(82) Slichter, C. P. *Principles of magnetic resonance, with examples from solid state physics*; Harper & Row: New York, 1963.

(83) Taulelle, F. *NMR of Quadrupolar Nuclei in the Solid State*; Kluwer Academic Publishers: London, 1988; Vol. 322, p 476.

(84) Haeberlen, U. *High resolution NMR in solids: selective averaging*; Academic Press: New York, 1976; p v.

(85) Mehring, M. *Principles of high-resolution NMR in solids*, 2nd ed.; Springer-Verlag: Berlin/ New York, 1983.

(86) Reif, B.; Jaroniec, C. P.; Rienstra, C. M.; Hohwy, M.; Griffin, R. G. *J. Magn. Reson.* **2001**, *151*, 320−327.

(87) Jaroniec, C. P.; MacPhee, C. E.; Astrof, N. S.; Dobson, C. M.; Griffin, R. G. *Proc. Natl. Acad. Sci. U. S. A.* **2002**, *99*, 16748−16753.

(88) Rienstra, C. M.; Tucker-Kellogg, L.; Jaroniec, C. P.; Hohwy, M.; Reif, B.; McMahon, M. T.; Tidor, B.; Lozano-Perez, T.; Griffin, R. G. *Proc. Natl. Acad. Sci. U. S. A.* **2002**, *99*, 10260−10265.

(89) Chopin, L.; Vega, S.; Gullion, T. *J. Am. Chem. Soc.* **1998**, *120*, 4406−4409.

(90) Goldbourt, A.; Vega, S.; Gullion, T.; Vega, A. J. *J. Am. Chem. Soc.* **2003**, *125*, 11194−11195.

(91) Vaneck, E. R. H.; Janssen, R.; Maas, W. E. J. R.; Veeman, W. S. *Chem. Phys. Lett.* **1990**, *174*, 428−432.

(92) Carroll, P. J.; Stewart, P. L.; Opella, S. J. *Acta Crystallogr., Sect. C: Cryst. Struct. Commun.* **1990**, *46*, 243−246.